Numerical Simulation of Electro-osmotic Flow Path Selection in a Y-Shaped Triangle

Corresponding Author:
Amir Heydari
Master's degree, mechanical engineering, energy conversion orientation, Payam Noor Khorasan Razavi University, Mashhad, Iran

ABSTRACT:
This research studied the switching process of an electroosmotic flow (EOF) in a Y-shape three-way microchannel by using analytical and numerical solutions. In the analytical study of the flow based on some proposed simplifying assumptions, equations were introduced to approximate the switching voltage ratio (λ) and EOF rate before and after the switching process. In the analyses, parameters "distance between outlet branches and the three-way" and "dimensionless thickness of the electrical double layer" were assumed to be flow variables, and their effects on the flow's ultimate condition were evaluated. Numerically, the Lattice Boltzmann method (LBM) and Poisson-Boltzmann approximation were used to solve all the equations governing the EOF in a two-dimensional Y-shape three-way microchannel. When comparing the analytical and numerical results, approximated equations of the analytical side possessed noticeably high accuracy and outperformed the numerical side in approximating the EOF rate at considerably lower computational efforts.

Keywords: Electroosmotic flow, Flow switching, Lattice Boltzmann

INTRODUCTION:

The electro-osmotic flow (EOF) inside microchannels is based on (and influenced by) the electrical double layer. When studying the behavior of an electrolyte solution, it can be seen that if the microchannel's solid walls are positioned adjacent to this solution, while the wall is charged, the electrostatic charges on the wall-fluid interface attract the counter ions and repel co-ions. As a result, the counter ions accumulate in the vicinity of the microchannel's wall and, thereby, form a layer termed the Stern layer, with a thickness of approximately less than 1 nm. Close to the Stern layer, there is a layer termed "Diffuse Layer" or "Gouy–Chapman" where the concentration of counter ions and co-ions on the wall is equal. The diffuse layer varies in thickness from a few nm to a few μm [1]. The electric potential at the solid-liquid interface is a key parameter in the arrangement of the charges.

In the literature, most studies on EOF have assumed a uniform charge density on the walls (*see, e.g., Yang et al. [2, 3], Zheng et al. [4], Kang et al. [5], Ren and Li [6]*). These studies advocate that the density of charge on the wall markedly influences the EOF characteristics. However, having a constant charge density on the wall is ideal, but difficult to attain in practice. Thus, the results of such research cannot be well matched with what happens in the real world. Some studies have explored the effects of the non-uniform distribution of surface charge on EOF. In their numerical and experimental research, for example, Ren and Lee [6] studied the EOF inside a circular

channel possessing axial changes of the surface charge. In a numerical study, Fou et al. [7] examined the effects of a step change in the surface area of the EOF and employed the Nernst-Planck equation to determine the concentration of ions in the EOF.

Some studies have numerically simulated the EOF using the Lattice Boltzmann Model (LBM). For example, Tang and Lee [8] analyzed the EOF in a flat microchannel under uniform and non-uniform surface charges. They proposed an LBM (*based on the thermal model of Hay et al. [9]*) to solve the Poisson-Boltzmann equation. The study by Tang and Lee was later expanded elsewhere to simulate the non-Newtonian EOF in a flat microchannel in the presence [10] and absence [11] of an external pressure gradient. Wang et al. [12] proposed a new LBM to solve the nonlinear Poisson-Boltzmann equation and used the proposed model to simulate an EOF in a flat microchannel [13], in a two-dimensional porous medium (under obstacles with the regular array) [14], and a three-dimensional porous medium (under obstacles with the irregular and stochastic array) [15]. Elsewhere, Wang et al. [16] studied how an EOF can be influenced by roughness and regular cavity on the surface of the wall. Likewise, Chai and Shi [17] simulated the EOF in a flat microchannel by proposing a new LBM with the Poisson-Boltzmann equation.

In the LBM, since the fluid and its model are assumed to be microscopic, the fluid flow is analyzed using the particle distribution function (PDF). Using a PDF that shows the potential presence of fluid particles in a

place allows the LBM to solve the simplified quasi-linear Boltzmann equation instead of solving the nonlinear Navier-Stokes equation. This considerably simplifies the formulation and enhances parallel processing. However, the LBM comes with some shortcomings, such as using the Cartesian grid and a larger number of unknowns compared to the Navier-Stokes equation. Due to these shortcomings, the boundary conditions of the PDFs have become a worth-exploring facet of the LBM.

A variety of boundary conditions have so far been proposed for the LBM in the solid-fluid interface, of which the Bounce-Back model is well established [18] and is a simple and accurate technique [19]. To improve the accuracy of this boundary condition, there are multiple ideas proposed, such as relocating the boundary from the node to the interface of two nodes [19], a bounce back on the non-equilibrium section [20], the thermodynamic equilibrium of distribution functions around the assumed velocity and density values [21], and the extrapolation of distribution functions [22].

Since the LBM is initially designed based on a Cartesian grid, the curvilinear boundaries of a hypothetical problem can maximally be proposed with a series of broken lines that challenge the physical integrity of the boundary and its peripheral flow. Despite its significance in solving the Boltzmann equation algorithm in the curvilinear coordinate system [23], the LBM's simplicity in the Cartesian grid has provoked researchers to run curvilinear boundaries in the Cartesian grid. Filippova and Hanel [23] are probably the first who model the curved boundary in the Cartesian grid using the Bounce-Back model and extrapolating the distribution functions proposed in [24]. This model is overwhelmed by instability, though this problem was then largely solved by Mei et al. [25, 26]. Bouzidi et al. [27] proposed a simpler boundary condition based on the Bounce-Back model to model the curved boundaries. This model merges the Bounce-Back model and extrapolation and is merely applicable to steady boundaries.

Using the Cartesian grid in the LBM allows the nodal grid not to unavoidably coincide with the curved boundary when hitting the curved boundaries. Under this condition, the distance between the boundary and the nodal points pivotally determines the equation governing the boundary condition, particularly when extrapolating or interpolating distribution functions. As such, there are two different equations governing the distribution function, and the unknown variable is variably proportioned to the distance of the curved boundary from the nodal points.

Due to its advantages over the other solvers of the Navier-Stokes equation, researchers mostly use the LBM to solve other nonlinear differential equations governing physical phenomena that can be used in overall geometries (e.g., curved boundaries) [28-30]. However, in most studies, curved boundary simulations are particularly conducted for fluid flow and relevant concepts [31-33].

In the microscopic boundary condition, the macroscopic property of extrapolation should be applied to the boundary points, which will differ based on the concerned physical phenomenon and its governing equation. For fluid flow and the Navier-Stokes equation, there is a new model proposed based on Zou et al. [34] that assigns a specific velocity to the boundary points. This model can be applied in all 2-D geometries and its design ensures no slip at nodal points.

Today, with the overuse of microsystems in biology, fuel cells, and laboratory chips, EOFs have become an effective way of fluid transfer. A leading flaw of common designs of electroosmotic micropumps is a need for very high voltages for pump running that can influence the flow contents. Takamura et al. [35] innovatively developed a cascade of low-voltage micro pumps to achieve the intended flow at a lower voltage.

The present research simulates an EOF inside a Y-shaped three-way microchannel and numerically investigates the switching process of the EOF and the parameters affecting this process. In the past, research has explored EOF control by the external electric field (EEF), but largely overlooked flow conditions before and after the switching process and its associated parameters. This research contains numerical and analytical analyses and compares the obtained results. The research is based on altering the voltage applied on the two ends of the microchannel and using electronic circuits, with no need for altering the flow medium. Thus, the fluid inside the microchannel is supposed to be under single-flow or full-flow conditions. In full-flow conditions, the electric field intensity and the EOF rate are equal for two branches of the microchannel. In turn, the EOF entering the microchannel is divided into two equal parts. In single-flow conditions, the EOF only passes through the top branch, and thereby, voltage and flow rate are equal to zero for the bottom branch. In this research, three variables associated with EOF in the microchannel are investigated: 1) flow rate in both branches in the full-flow condition, 2) voltage ratio (λ) required to stop EOF in the bottom branch, and convert the full-flow condition to the single-flow condition, and 3) flow rate in the top branch in the single-flow condition. Parameters k and α play a key role in the EOF rate and switching process. Furthermore, based on the study by Mohammadi Pour et al., this research uses equations governing EOF (i.e., continuity, Navier-Stokes, Laplace, and Poisson-Boltzmann) to solve the Poisson equation governing the electric potential.

EOF simulation using the LBM and analysis of the results

Geometry of the problem

Three flat microchannels (each with a thickness of 30 μm a length of 90 μm) are connected by a Y-shaped three-way (Figure 1). The developed assembly (210 μm in length) is adjacent to an electrolyte with ion number density (n_0) and dielectric constant (r^ε).

Under this geometry, the walls are charged by ξ. The distance (d) between the two right walls, which here are termed top and bottom branches, respectively, is set at 30, 60, 90, 120, and 150 μm. The surface charge on the microchannel walls alters the ionic arrangement in the electrolyte and forms an electrical double layer, ultimately forming an internal electric field in the vicinity of the walls.
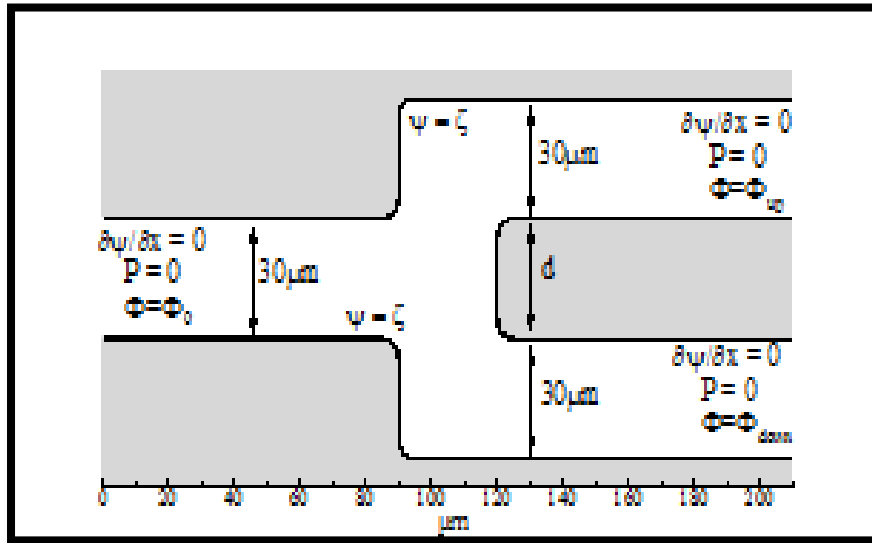

Figure 1. Geometry and boundary conditions for EOF through a Y-shaped three-way channel

Governing macroscopic equations

Based on the electric field theory, a Poisson equation correlates electric potential distribution (ψ) in electrolyte adjacent to the wall (Ψ) to the net electric charge density (ρe). In an electrolyte, "ρe" is proportional to the numerical concentration of positive and negative ions [$\rho e = ze(n^+ - n^-)$], where the concentration of these ions is obtained by solving the Nernst–Planck equation.

As shown in Figure 1, the surface charge remains constant along the walls, indicating a significant alteration in ion concentration only in the direction perpendicular to the surface (β). Here, the Nernst–Planck equation is simplified as follows:

$$\frac{1}{n^{\pm}}\frac{dn^{\pm}}{d\beta} + \frac{z^{\pm}e}{k_bT}\frac{d\psi}{d\beta} = 0 \tag{1}$$

When integrating Eq. (1), assuming a point in the center of the channel where ions are naturally distributed and their concentration is equal to the mass density (ρe) and electric potential ($\psi = 0$), the Boltzmann distribution will be as follows:

$$n^{\pm} = n_0 \exp\left(\frac{-z^{\pm}e\psi}{k_bT}\right) \tag{2}$$

This microchannel is adjacent to an electrolyte with an ion number density of (n_0) and dielectric constant of (ε_w). The surface charge on the microchannel walls alters the ionic arrangement in the electrolyte and forms an electrical double layer, ultimately forming an internal electric field in the vicinity of the walls. Based on the electric field theory, a Poisson equation correlates electric potential distribution (ψ) in

electrolyte adjacent to the wall (Ψ) to the net electric charge density (ρe) [36].

By introducing the dimensionless rarefaction as ($x^* = \frac{x}{h}, y^* = \frac{y}{h}, \Psi^* = ze\psi, \rho_e^* = \rho e/(zen_0)$), and after removing the superscript (*) for simplicity, the Poisson equation governing the potential will be as follows:

$$\frac{\partial^2 \psi}{\partial x^2} + \frac{\partial^2 x}{\partial y^2} = -\frac{k^2 \rho_e}{2} \tag{3}$$

Where ($\kappa = KH$) is the dimensionless thickness of the electrical double layer and ($k = \left(2z^2c^2n_0 / \left[\varepsilon_r\varepsilon_o k_bT\right]\right)^{0.5}$) is the Debye-Huckel parameter. Regarding the boundary conditions of this equation (as shown in Figure 1), ($\Psi = \zeta$) is the known values of walls, and variation in the electric potential gradient at the inlet and outlet of the microchannel is ($\frac{\partial^2 \Psi}{\partial x^2} = 0$).

(Φ) is the dimensionless external electric potential generated upon applying an EEF in two ends of the microchannel. After removing the superscript (*) for simplicity, it follows the Laplace equation below [36]:

$$\frac{\partial^2 \phi}{\partial x^2} + \frac{\partial^2 \phi}{\partial y^2} = 0 \tag{4}$$

The boundary conditions of the external electric potential are constant values of $\emptyset_{Right} = 0$ and $\emptyset_{Left} = E_xL$ at both ends of the microchannel, and the normal gradient in walls is zero ($\frac{\partial \phi}{\partial m} = 0$), where m is perpendicular to the boundary. Applying an EEF in the microchannel will accumulate the ions close to the

charged wall, thereby enforcing the fluid. Applying this volumetric force in the momentum equation will generalize the Navier-Stokes equation as follows:

$$v_x \frac{\partial v_x}{\partial x} + v_y \frac{\partial v_x}{\partial y} = -\frac{\partial p}{\partial x} + \frac{1}{Re}\left(\frac{\partial^2 v_x}{\partial x^2} + \frac{\partial^2 v_x}{\partial y^2}\right) - B\rho_e\left(\frac{\partial \psi}{\partial x} + A\frac{\partial \phi}{\partial x}\right)$$

$$v_x \frac{\partial v_y}{\partial x} + v_y \frac{\partial v_y}{\partial y} = -\frac{\partial p}{\partial y} + \frac{1}{Re}\left(\frac{\partial^2 v_y}{\partial x^2} + \frac{\partial^2 v_y}{\partial y^2}\right) - B\rho_e\left(\frac{\partial \psi}{\partial y} + A\frac{\partial \phi}{\partial y}\right)$$

(5)

Where B $= n_0 k_b T/(\rho u_{eo}^2)$ is the ionic pressure to dynamic pressure ratio. The no-slip condition governs the walls, and the pressure at both ends of the microchannel is set at zero, in line with the working conditions of most laboratory chips [37].

The boundary conditions of the problem

Regarding the boundary conditions of this equation (as shown in Figure 1), ($\varsigma = \psi$) is the known values of walls, and variation in the electric potential gradient at the inlet and outlet of the microchannel is ($\frac{\partial \psi}{\partial x} = 0$).

The EEF (Φ) is applied through electrodes to both ends of the microchannel. The distribution of this field inside the microchannel follows the Laplace equation. The EEF's boundary conditions are as constant values of Φ (at inlet), Φ_{up} at the end of the top branch, Φ_{down} at the end of the bottom branch, and normal gradient of zero ($\frac{\partial \phi}{\partial x} = 0$) on walls. Applying an EEF in the microchannel will accumulate the ions close to the charged wall, thereby enforcing the fluid. Applying this volumetric force in the momentum equation will generalize the Navier-Stokes equation. In this research, the EOF path is determined by altering the intensity of voltage applied at both ends of the microchannel. For this, the EOF is considered to be either single or full.

Analysis of the full EOF

Under this condition, the same voltage ($\Phi_{down} = \Phi_{up} = 0$) is applied to the end of both branches, while the voltage applied to the inlet of the microchannel equals ($\Phi_0 = E_{ref}L$), where L is the distance between both ends and is 210 μm. Under this condition, the EEF's intensity is equal in both branches and, thereby, both branches convey the same rate of EOF. In turn, the inlet flow is divided into two equal parts when approaching the three-way to leave the solving space through branches.

Analysis of the single EOF

Under this condition, the EOF only passes through the top branch. However, due to geometric symmetry, the results can also be generalized to the bottom branch. Here, the voltage at the end of the top branch and inlet of the microchannel equals respectively to ($\Phi = -E_{ref}L, \Phi_{up} = 0$). To achieve a single EOF, the voltage at the end of the bottom branch should be adjusted to attain an EOF rate of zero in this branch. This voltage (λ) is shown proportional to the inlet voltage as follows:

$$\frac{\Phi_{down}}{\Phi_0} = \lambda$$

(6)

This research aims to approximate three fundamental quantities of the EOF passing the three-way: 1) EOF rate in both branches in the full condition, 2) voltage ratio (λ) required to stop EOF in the bottom branch and convert full condition to single condition, and 3) flow rate in the top branch in the single condition.

Approximate analytical solution

The EOF simulation by solving the governing equations is discussed in the next section. However, solving the governing equations needs huge computational efforts, particularly when it comes to the design of micro-electromechanical systems.

The aim, here, is to attain an analytical solution to approximate single and full EOF conditions by defining some assumptions. Before introducing these assumptions, first suppose an EOF in a flat and straight microchannel that conveys an EOF that is highly developed in terms of ion density, velocity, and electric potential. Also, the electrical double layers on both sides of the microchannel do not interfere. Suppose the walls' surface charge is uniform along the microchannel's length and the corresponding electric potential is less than 30 mV, then solving the governing culminates in the velocity profile below [6]:

$$u(y) = -\frac{\varepsilon_r \varepsilon_0 E_x \zeta}{\mu}\left[1 - \frac{\cosh(ky - kH/2)}{\cosh(kH/2)}\right]$$

(7)

Eq. (7) is a "precise" analytical representation of the flow conditions in a straight microchannel. The approximation here is to apply Eq. (6) to the straight parts of the concerned geometry (Figure 1). Thus, Eq. (7) can be rewritten as follows, based on the definitions of dimensionless rarefaction:

$$u(y) = \frac{u}{u_{ref}} = -\frac{E}{E_{ref}}\left[1 - \frac{\cosh(ky - kH/2)}{\cosh(kH/2)}\right]$$

(8)

In the straight microchannel, the EEF's intensity (E) and the reference field (E_{ref}) are equal. Thus, the term (E/E_{ref}) in a microchannel is equal to the reference field and Eq. (8) is the dimensionless form of Eq. (8). However, in the concerned geometry, the EEF's intensity in each of the microchannel's straight sections can differ from the reference EEF's intensity. Other assumptions to attain the analytical solution are as follows:

- Regardless of the flow conditions where the flow direction alters due to geometrical changes, the EOF's condition (separately) in entry and branches is nearly developed and supposed to be uniform.
- The effects of change in pressure due to EOF direction change are overlooked.

By assuming degrees of error for the above assumptions, the EOF will be analytically studied around four key sections shown in Figure 2: Section A (at the microchannel entry), Section B (at the center of the microchannel), Section C (at the entry of the top branch), and Section D (at the end of the top branch).

Likewise, sections E and F can be defined for the bottom branch, corresponding to sections C and D (in the top branch). In the rest of this article, all the quantities of these sections or their intermediates are denoted by relevant subscripts.
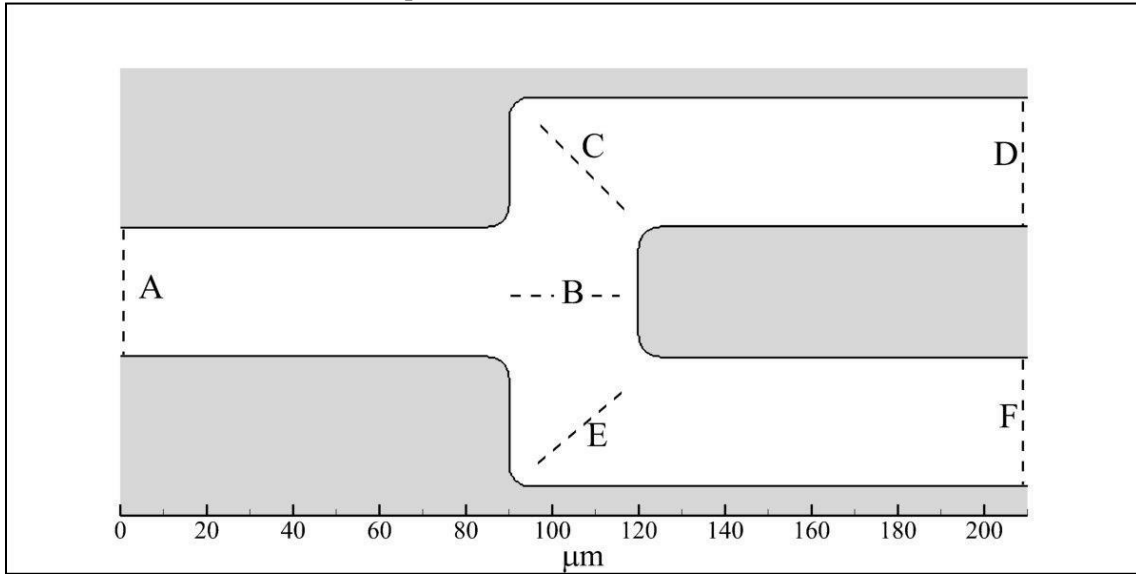

Figure 2. Sections in the approximate analytical solution of an EOF in a Y-shaped three-way microchannel

Note that each parameter that influences the reference velocity (e.g., surface charge, dielectric constant, etc.,) will also influence the EOF's ultimate condition. However, to maintain the results to be generalizable, we discuss dimensionless variables, such as voltage ratio (λ), dimensionless flow rate (Q^*), and dimensionless distance between branches ($\alpha = \dfrac{d}{H}$).

Analysis of full EOF by the equivalent electric circuit
Since a Laplace equation governs the external electric potential, we can use the equivalent circuit theory to quantify the EOF intensity in the microchannel's straight sections [38]. Based on this theory, the microchannels that convey an EEF are modeled as a resistance proportional to the microchannel's length (L) and inverse of its width (H) ($R = \dfrac{L}{H}$). The geometry shown in Figure 2 will be approximated with a similar electric circuit shown in Figure 3. This approximation supposes the EEF to change one-dimensionally. Obviously, this approximation fails to elucidate transverse variations in the EEF, particularly where the direction alters. However, based on the above assumptions, we can use an equivalent circuit regardless of transverse variations in the EEF's intensity.
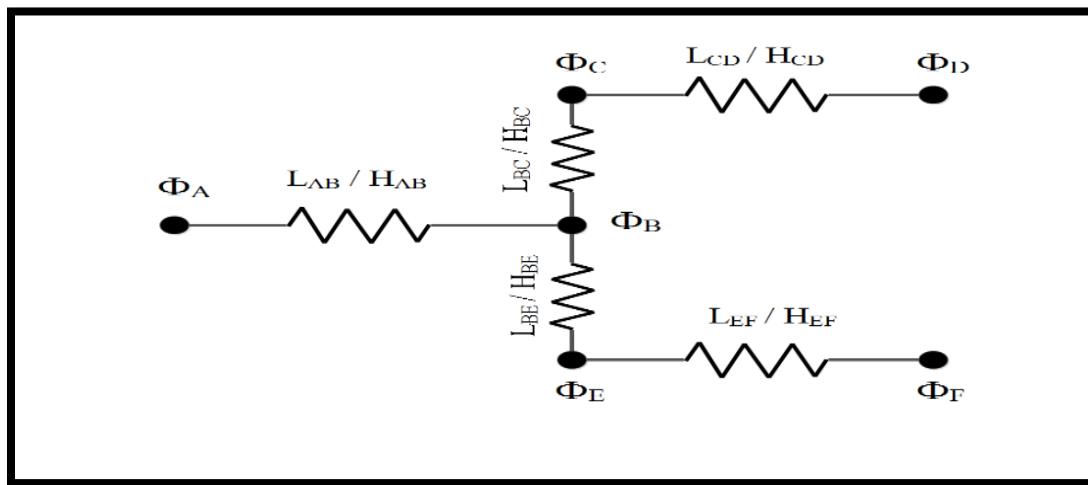

Figure 3. The equivalent electrical circuit used to calculate EEF for full-flow condition

For the geometry shown in Figure 1, the following geometrical equations are established:

$$H_{AB} = H_{BC} = H_{CD} = H_{BE} = H_{EF} = H$$

$$L_{AB} = L_{CD} = L_{EF} = 3.5H$$

$$L_{BC} = L_{BE} = (H + d)/2 = (1 + \alpha)H/2 \qquad \alpha = 1, 2, 3, 4, 5$$

By solving the electrical circuit given in Figure 3, the EEF's intensity in the AB part is calculated as follows:

$$E_{AB} = \frac{\phi_B - \phi_A}{L_{AB}} \approx \frac{28}{22+\alpha} E_{ref} \quad (9)$$

Using "≈" instead of "=" in Eq. (9) and the following equations implies that the extracted equations are based on a set of simplifying assumptions. By incorporating Eq. (9) in Eq. (8) and then integrating it, the EOF rate in the AB part will be quantified.

The EOF rate is similar for both branches for the full-flow condition, as follows:

$$Q^*_{up} = Q^*_{down} \approx \frac{14}{22+\alpha}\left(1 - \frac{\tanh(k/2)}{k/2}\right) \quad (10)$$

Analysis of single EOF by the equivalent electric circuit

In the single flow condition, the EOF rate in the branch is zero. To attain this condition, the EEF's intensity needs to be zero. In turn, the voltage applied at the end of this branch (Φ_{down}) should be equal to ($_B\Phi$). This equivalent electrical circuit in the single-flow condition is depicted in Figure 4.
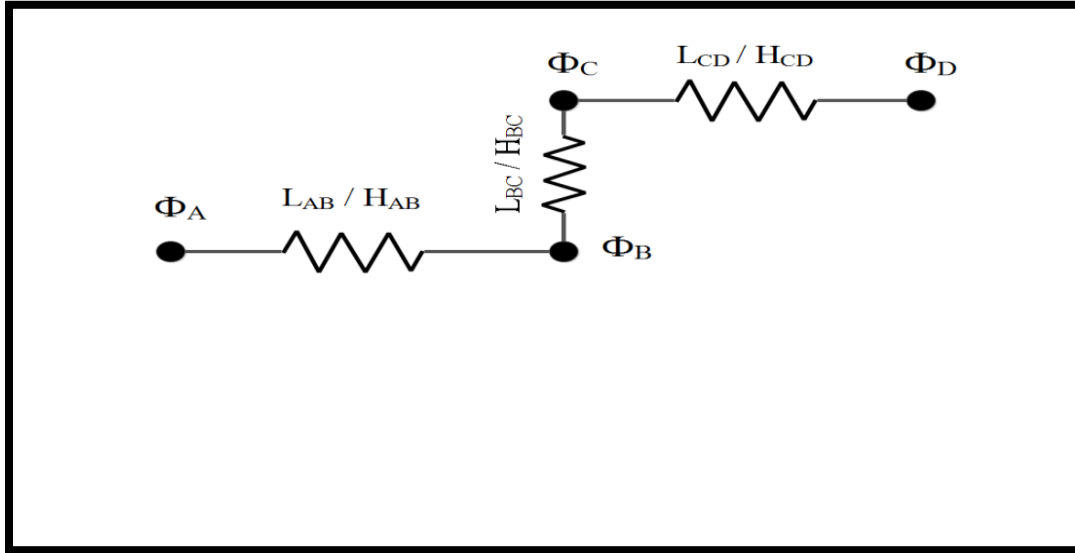

Figure 4. The equivalent electrical circuit used to calculate EEF for single-flow condition

By solving the equivalent electrical circuit (Figure 4), the voltage ratio required to stop EOF in the bottom branch is calculated from Eq. (11):

$$\lambda = \frac{\phi_{down}}{\phi_0} \approx \frac{\phi_B}{\phi_A} = \frac{8+\alpha}{15+\alpha} \quad (11)$$

In this condition, the EEF's intensity in the AB part is as follows:

$$E_{AB} = \frac{\phi_B - \phi_A}{L_{AB}} \approx \frac{14}{15+\alpha} E_{ref} \quad (12)$$

By incorporating Eq. (12) in the velocity distribution equation (Eq. 13), the EOF rate at the inlet and in the top branch is obtained as follows (note that, all the EOF is conveyed through the top branch):

$$Q^*_{up} = Q^*_{in} \approx \frac{14}{15+\alpha}\left(1 - \frac{\tanh(k/2)}{k/2}\right) \quad (13)$$

Findings
Detection and analysis of voltage ratio (λ) for EOH switching

In this research, the flow bed is assumed to be of the same material. Thus, the surface charge due to the vicinity to the electrolyte is constant on all the surfaces and equals to (ζ). Figure 5 depicts the distribution of the internal electric field under this surface charge. Table 1 presents fluid parameters and properties used in the simulation.
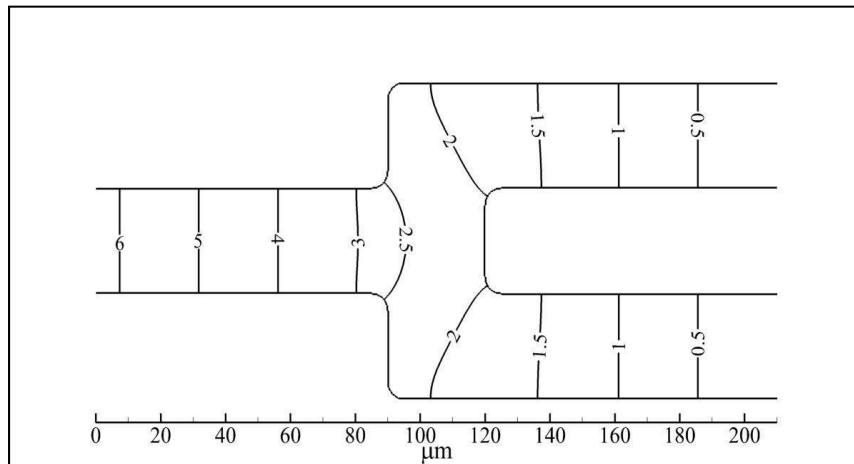

Figure 5. Distribution of electric field caused by the presence of electrodes at both ends of the microchannel

Table 1. Constants and properties of the fluid in EOF simulation	
Parameter	Value (unit)
k	5.15
α	1, 2, 3, 4, 5
ε_r	80
ζ	-25 (mV)
E	-30 (V/mm)
ρ	1×10^3 (kg/m^3)
μ	1×10^{-3} (Pa.s)

Dimensionless contour lines (Φ) in full-flow condition are shown in Figure 5 for α = 1. As shown, the distribution of contour lines (Φ) changes one-dimensionally in the microchannel's inlet and both branches, but it changes two-dimensionally in the interface of both branches, at the distance of 90 to 120 μm. As depicted in Figure 5, variations in EEF intensity ($\nabla\Phi$) differ between the microchannel's inlet and the outlet branches, with variations in Φ values in the inlet area that are almost twice that in the outlet branches. We can easily justify this change with the equivalent electric circuit.

Determination of EOF velocity and rate in full-flow condition

By using the results of EEF (Φ) and internal electric field (ψ) in the flow solution, the velocity field in the full-flow conditions is based on Figure 6. As shown, under this condition, the same volume of flow passes through both branches, where each branch conveys half of the inlet flow.
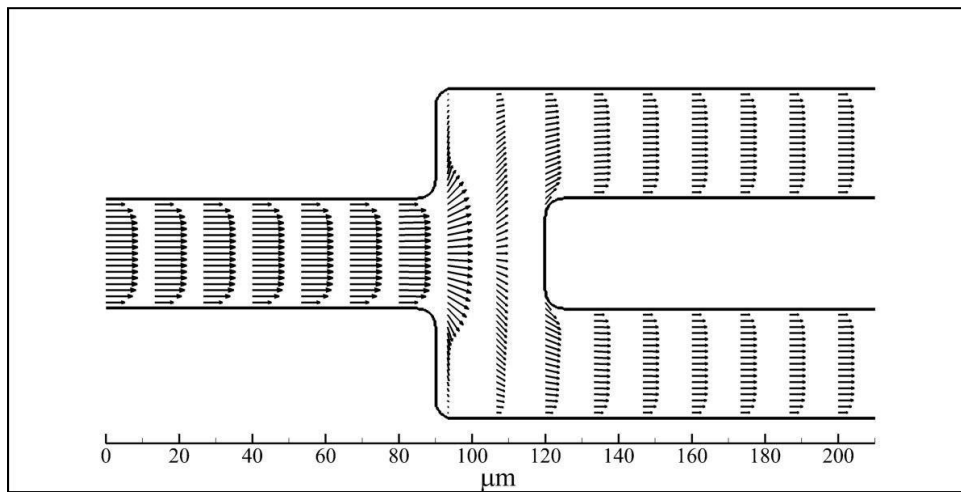

Figure 6. Velocity vectors in full-flow condition for $k = 15$ and $\alpha = 1$

If increasing the boundary condition for voltage in the bottom branch with $0.2\emptyset$ steps, and continuing simulation in each step to attain a steady state, then the flow rate at the inlet (Q_{in}), top branch (Q_{top}), and bottom branch (Q_{down}) will be calculated by integrating velocity distribution in each step.
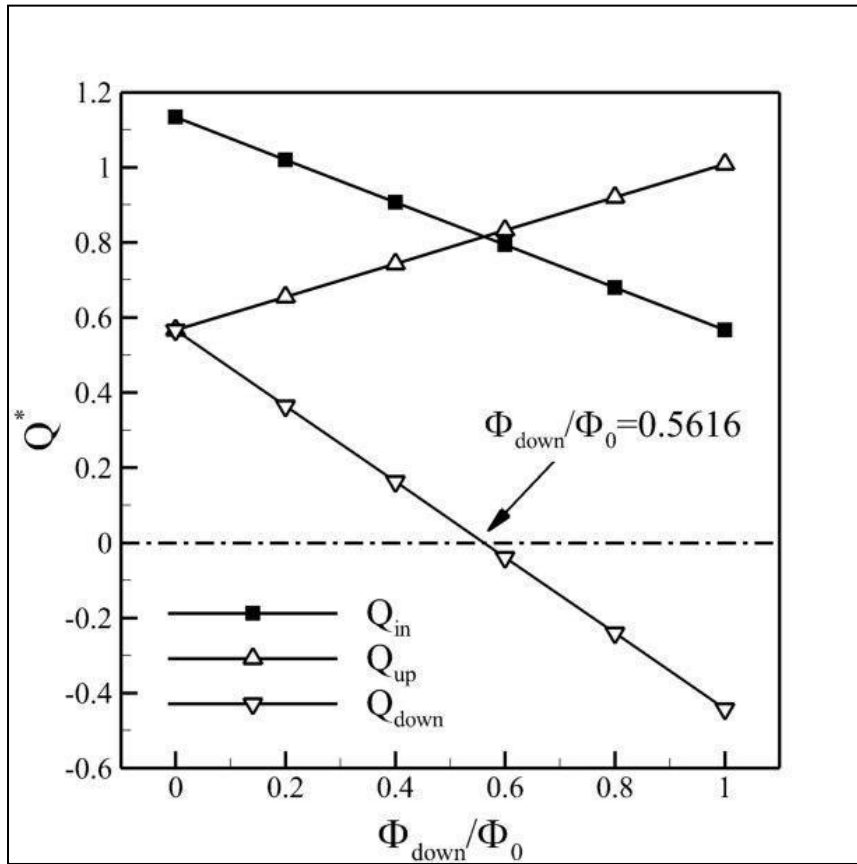
Figure 7. Variations in flow rate for varying voltage at the end of bottom branch for $k = 15$ and $\alpha = 1$

As shown in Figure 7, ($\dfrac{\Phi_{down}}{\Phi_0} = 0$) is the same for the EOF passing the branches and equals half the inlet flow rate. By increasing the voltage ratio ($\dfrac{\Phi_{down}}{\Phi_0}$), the flow rate is reduced in the bottom branch and increased in the top branch. These changes ultimately reduce the inlet flow rate. Considering linear changes in flow rate for variations in the voltage ratio, we can calculate the voltage ratio (λ) required to stop EOF in the bottom branch by interpolation.

Having $\lambda = 0.5616$, as shown in Figure 7 (for $k = 15$ and $\alpha = 1$), with a rise in λ, the flow rate will be negative in the bottom branch, indicating reverse flow pumping in this branch. Now, λ is determined, but it requires further validation by re-simulating flow condition with the following boundary conditions:

$$\Phi_0 = -E_{ref}L, \Phi_{up} = 0, \Phi_{down} = \lambda\Phi_0$$

Figure 8 shows the distribution of the electric field due to the boundary condition, where variations in Φ in the bottom branch are zero. Thus, no volumetric force is applied to the flow when the internal electric field is adjacent to this branch.
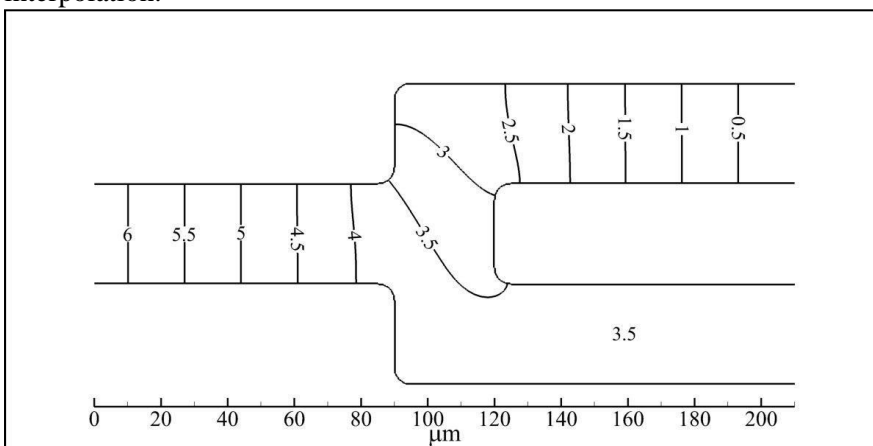

Figure 8. Dimensionless contour lines in the single-flow condition for $\alpha = 1$

Determination of flow velocity and rate in the single-flow condition
Figure 9 demonstrates velocity distribution in the single-flow condition. As shown, by applying the value of λ obtained from interpolation, the flow rate in the bottom branch is zero. Thus, the λ value obtained through interpolation is true and considered the numerical analysis result.
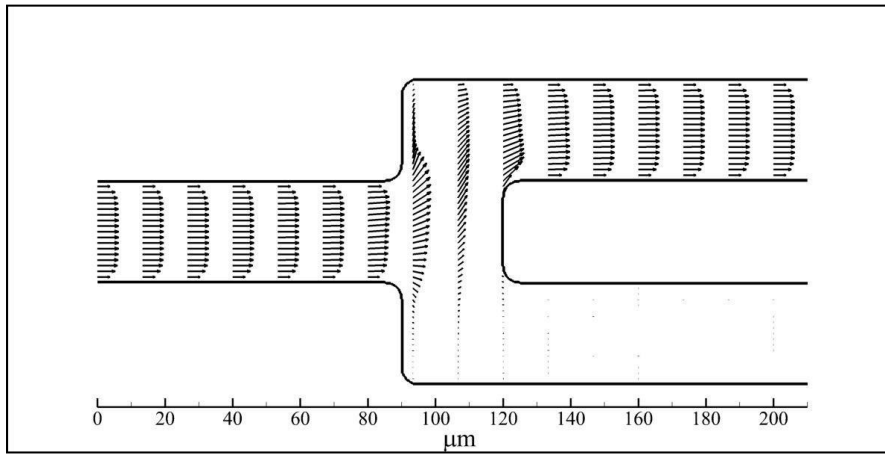
Figure 9. Velocity vectors in the single-flow condition for $k = 15$ and $\alpha = 1$

Table 2 presents values obtained from numerical simulation and approximate solving.

Table 2. The λ value required to stop EOF in the bottom branch			
α	$\lambda \, (k = 15)$	$\lambda \, (k = 15)$	$\lambda \, (15)$
1	0.5616	0.5612	0.5625
2	0.5914	0.5886	0.5882
3	0.6160	0.628	0.6111
4	0.6375	0.6340	0.6316
5	0.6566	0.6532	0.6500

As given in Table 3, the flow rate in the top branch is investigated for full-flow and single-flow conditions.

Table 3. EOF rate in the top branch in the full-flow condition for $k = 5$			
α	Numerical solution (Q_{up})	$Q_{up}(14)$	Error (%)
1	0.3920	0.3685	6.0
2	0.3730	0.3531	5.3
3	0.3571	0.3390	5
4	0.3429	0.3260	4.9
5	0.3295	0.3139	4.7

Tables 4 to 6 compare the results of numerical simulation with the results for dimensionless parameters of the electrical double layer thickness for k = 5 and k = 15.

Table 4. EOF rate in the top branch in the single-flow condition for $k = 5$			
α	Numerical solution (Q_{up})	$Q_{up}(17)$	Error (%)
1	0.5640	0.5297	6.1
2	0.5264	0.4985	5.3
3	0.4953	0.4708	4.9
4	0.4683	0.4461	4.7
5	0.4440	0.4237	4.5

Table 5. EOF rate in the top branch in the full-flow condition for $k = 15$			
α	Numerical solution (Q_{up})	$Q_{up}(14)$	Error (%)
1	0.5667	0.5275	6.9
2	0.5428	0.5056	6.9
3	0.5203	0.4853	6.7
4	0.4992	0.4667	6.5
5	0.4796	0.4494	6.3

Table 6. EOF rate in the top branch in the single-flow condition for $k = 15$			
α	Numerical solution (Q_{up})	$Q_{up}(17)$	Error (%)
1	0.8151	0.7583	7
2	0.7646	0.7137	6.7
3	0.7201	0.6741	6.4
4	0.6802	0.6386	6.1
5	0.6443	0.6067	5.8

With a maximum error of 7%, the results can accurately predict the flow rate in the branch under full-flow and single-flow conditions. Furthermore, a reduction in relative error occurs when the distance between the two branches (α value) is increased. This behavior can be attributed to the assumptions defined when extracting the equations, where the flow in each interface is considered to be one-dimensional. With increasing α and as the branches approach each other, the flow will be highly two-dimensional in the three-way, whereas the one-dimensional approximation error will increase.

Conclusion

This research analytically and numerically studied the switching process of an EOF in a Y-shaped three-way microchannel. Analytically, by introducing some assumptions, the flow in the straight part of the three-way was supposed to be one-dimensional. By using the equivalent electric circuit theory, an approximate solution was extracted for the voltage ratio and the flow rate in the branches before and after the switching process. Next, the flow condition was simulated by numerically solving the governing equations and recalculating the intended parameters. When comparing the numerical and approximate results, it was found that the approximate solution is accurate in predicting the voltage ratio needed for the switching process and calculating the flow rate passing through the branch before and after the switching process. Due to the low computational effort required and high accuracy, approximate solutions outperform numerical solutions to solve governing equations and, thereby can be viewed as potent tools in designing micro-electromechanical systems.

References

1. Chapter 4 Electroosmotic flows in microchannels," in *Interface Scienc Technology*. vol. Volume 2, L. Dongqing, Ed., ed: Elsevier, 2004, pp. 92-20 .

2. Yang R. J., Tseng T. I., and Chang C. C., "End effects on electro-osmotic flows in microchannels" Journal of Micromechanics and Microengineering, Vol. 15, No. 2, 2005, pp. 254-262.

3. Ren L., and Li D., "Theoretical Studies of Microfluidic Dispensing Processes" Journal of colloid and interface science, Vol. 254, No. 2, 2002, pp. 384-395.

4. Zhang Y., Gu X. J., Barber R. W., and Emerson D. R., "An analysis of induced pressure fields in electroosmotic flows through microchannels" Journal of colloid and interface science, Vol. 275, No. 2, 2004, pp. 670-678.

5. Kang Y., Yang C., and Huang X., "Dynamic aspects of electroosmotic flow in a cylindrical microcapillary" International Journal of Engineering Science, Vol. 40, No. 20, 2002, pp. 2203- 2221.

6. Ren L., and Li D., "Electroosmotic Flow in Heterogeneous Microchannels" Journal of colloid and interface science, Vol. 243, No. 1, 2001, pp. 255-261.

7. Fu L., Lin J.-Y., and Yang R.-J., "Analysis of electroosmotic flow with step change in zetapotential" Journal of colloid and interface science, Vol. 258, No. 2, 2003, pp. 266-275.

8. Tang G. H., Li Z., Wang J. K., He Y. L., and Tao W. Q., "Electroosmotic flow and mixing in microchannels with the lattice Boltzmann method" J. Appl. Phys., Vol. 100, No. 9, 2006, pp. 094908.

9. He X., Chen S., and Doolen G. D., "A Novel Thermal Model for the Lattice Boltzmann Method in Incompressible Limit" Journal of Computational Physics, Vol. 146, No. 1, 1998, pp. 282-300.

10. Tang G. H., Ye P. X., and Tao W. Q., "Pressure-driven and electroosmotic non-Newtonian flows through microporous media via lattice Boltzmann method" J. Non-Newton. Fluid Mech., Vol. 165, No. 21-22, 2010, pp. 1536-1542.

11. Tang G. H., Li X. F., He Y. L., and Tao W. Q., "Electroosmotic flow of non-Newtonian fluid in microchannels" Journal of Non-Newtonian Fluid Mechanics, Vol. 157, No. 1-2, 2009, pp. 133- 137.

12. Wang J., Wang M., and Li Z., "Lattice evolution solution for the nonlinear Poisson–Boltzmann equation in confined domains" Commun. Nonlinear Sci., Vol. 13, No. 3, 2008, pp. 575- 583.

13. Wang J., Wang M., and Li Z., "Lattice Poisson-Boltzmann simulations of electro-osmotic flows in microchannels" J. Colloid Interface Sci., Vol. 296, No. 2, 2006, pp. 729-736.

14. Wang M., Wang J., Chen S., and Pan N., "Electrokinetic pumping effects of charged porousmedia in microchannels using the lattice Poisson-Boltzmann method" J. Colloid Interface Sci., Vol.304, No. 1, 2006, pp. 246-253.

15. Wang M., and Chen S., "Electroosmosis in homogeneously charged micro- and nanoscale random porous media" J. Colloid Interface Sci., Vol. 314, No. 1, 2007, pp. 264-273.

16. Wang M., Wang J., and Chen S., "Roughness and cavitations effects on electro-osmotic flows in rough microchannels using the lattice Poisson–Boltzmann methods" J. Comput. Phys., Vol. 226, No. 1, 2007, pp. 836-851.

17. Chai Z., and Shi B., "Simulation of electro-osmotic flow in microchannel with lattice Boltzmann method" Phys. Lett. A Vol. 364, No. 3-4, 2007, pp. 183-188.

18. Ziegler D. P., "Boundary conditions for lattice Boltzmann simulations" J. Stat. Phys., Vol. 71, No. 5-6, 1993, pp. 1171-1177.

19. He X., Zou Q., Luo L.-S., and Dembo M., "Analytic solutions of simple flows and analysis of nonslip boundary conditions for the lattice Boltzmann BGK model" J. Stat. Phys., Vol. 87, No. 1-2, 1997, pp. 115-136.

20. Zou Q., and He X., "On pressure and velocity boundary conditions for the lattice Boltzmann BGK model" Phys. Fluids, Vol. 9, No. 6, 1997, pp. 1591.

21. Inamuro T., Yoshino M., and Ogino F., "A non-slip boundary condition for lattice Boltzmann simulations" Phys. Fluids, Vol. 7, No. 12, 1995, pp. 2928.

22. Chen S., Martínez D., and Mei R., "On boundary conditions in lattice Boltzmann methods" Phys. Fluids, Vol. 8, No. 9, 1996, pp. 2527.

23. Filippova O., and Hänel D., "Boundary-Fitting and Local Grid Refinement for Lattice-BGK Models" Int. J. Mod. Phys. C, Vol. 09, No. 08, 1998, pp. 1271-1279.

24. Chen S., Martínez D., and Mei R., "On boundary conditions in lattice Boltzmann methods" Phys. Fluids, Vol. 8, No. 9, 1996, pp. 2527.

25. Mei R., Luo L.-S., and Shyy W., "An Accurate Curved Boundary Treatment in the Lattice Boltzmann Method" J. Comput. Phys., Vol. 155, No. 2, 1999, pp. 307-330.

26. Mei R., Shyy W., Yu D., and Luo L.-S., "Lattice Boltzmann Method for 3-D Flows with Curved Boundary" J. Comput. Phys., Vol. 161, No. 2, 2000, pp. 680-699.

27. Bouzidi M. h., Firdaouss M., and Lallemand P., "Momentum transfer of a Boltzmann-lattice

fluid with boundaries" Phys. Fluids, Vol. 13, No. 11, 2001, pp. 3452.

28. Chai Z., and Shi B., "Simulation of electro-osmotic flow in microchannel with lattice Boltzmann method" Phys. Lett. A Vol. 364, No. 3-4, 2007, pp. 183-188.

29. Wang J., Wang M., and Li Z., "Lattice evolution solution for the nonlinear Poisson–

30. Tang G. H., Li Z., Wang J. K., He Y. L., and Tao W. Q., "Electroosmotic flow and mixing in microchannels with the lattice Boltzmann method" J. Appl. Phys., Vol. 100, No. 9, 2006, pp. 094908.

31. Yu D., Mei R., Luo L.-S., and Shyy W., "Viscous flow computations with the method of lattice Boltzmann equation" Prog. Aerosp. Sci. , Vol. 39, No. 5, 2003, pp. 329-367.

32. Kao P. H., and Yang R. J., "An investigation into curved and moving boundary treatments in the lattice Boltzmann method" J. Comput. Phys., Vol. 227, No. 11, 2008, pp. 5671-5690.

33. Verschaeve J. C. G., and Müller B., "A curved no-slip boundary condition for the lattice Boltzmann method" J. Comput. Phys., Vol. 229, No. 19, 2010, pp. 6781-6803.

34. Zou Q., and He X., "On pressure and velocity boundary conditions for the lattice Boltzmann BGK model" Phys. Fluids, Vol. 9, No. 6, 1997, pp. 1591.

35. Takamura Y., Onoda H., Inokuchi H., Adachi S., Oki A., and Horiike Y., "Low-voltage electroosmosis pump for stand-alone microfluidics devices" Electrophoresis, Vol. 24, No. 1-2, 2003, pp. 185-192.

36. Probstein R. F., Physicochemical hydrodynamics : an introduction, Wiley, New York, 1994.

37. Dutta P., Beskok A., and Warburton T. C., "Numerical Simulation of Mixed Electroosmotic/Pressure Driven Microflows" Numer. Heat Tr. A-Appl, Vol. 41, No. 2, 2002, pp. 131-148

38. R. Sun, C.-O. Ng, Effective slip for flow through a channel bounded by lubricant-impregnated grooved surfaces, *Theoretical and Computational Fluid Dynamics,* Vol. 31, No. 2, pp. 189-209, 2017.